JOURNAL OF MATERIALS SCIENCE 33 (1998) 5221–5228

Analysis of the single-fiber fragmentation test

S. LEE*, T. NGUYEN‡, J. CHIN, T.-J. CHUANG
National Institute of Standards and Technology, Gaithersburg, MD 20899 USA

An analysis of the single-fiber fragmentation test was investigated. An approximate solution for the stress fields of a fiber embedded in a polymer matrix of different elastic moduli was obtained by the Eshelby method. The fiber was modeled as a prolate spheroid. The axial stress of the fiber increases with increasing aspect ratio and fiber-matrix shear modulus ratio and decreases with increasing matrix and fiber Poisson's ratios. Using this analysis, the fracture stress of a single-fiber fragmentation specimen was derived. The applied stress at fiber fracture decreases monotonically with increasing aspect ratio of the fragmented fiber and increases with increasing fiber and matrix Poisson's ratios. This model is in qualitative agreement with published experimental data.

1. Introduction

Fiber-reinforced polymeric composites have been widely used in machines and structures because of their combination of low weight and high strength. One method commonly used for characterizing the interfacial strength between a fiber and the surrounding matrix is the single-fiber fragmentation test. In this technique, a fiber is embedded in a polymer matrix coupon and a tensile load is applied to the coupon. With increasing load, the fiber fractures into shorter and shorter fragmentations until the shear stress transfer across the interface is insufficient to cause further fracture of the fiber. The interfacial shear stress is then estimated from the fragment length distribution [1–8]. Because of the random nature of fiber fracture, the critical fragmentation aspect ratio was widely analyzed using the Weibull distribution [2–8]. Mai and co-workers [7, 8] used the Weibull probability of failure to predict the average tensile strength of a fiber. The Weibull probability was also applied to carbon fibers [9].

The single-fiber fragmentation test was originally proposed by Kelly and Tyson [1] for brittle fibers embedded in a copper matrix. The applicability of this technique for measuring the interfacial properties of polymer/fiber composites has been verified experimentally by Schultz and Nardin [10, 11]. They found that the fiber/matrix shear strength obtained by the single-fiber fragmentation test is linearly proportional to the reversible work of adhesion between the two materials for a wide variety of polymer/fiber composites. Since its inception, several studies have been performed to analyze the stress distribution within and near the fibers in polymer composites. Cox [12] used a shear lag model to analyze the stress state near a broken fiber end. Whitney and Drzal [13] proposed an analytical model to calculate the stress distribution near a broken fiber based on the superposition of an exact far-field solution and approximate transient solution. Liu *et al*. [14] applied computer simulation to describe the fragmentation process of the fiber in a single-fiber composite. Mai and co-workers [7, 8, 15] studied the fiber-reinforced composites with regard to the matrix-fiber interface conditions: full bonding, partial debonding, and full frictional bonding. Gent and Wang [16] and Liu *et al*. [17] addressed the effect of realistic problems, such as fiber cracking and interfacial debonding, in their analyses.

Treatments of fibers as elastic inclusions have been studied. Selvadurai and Rajapakse [18] considered a rigid cylindrical inclusion embedded in an elastic half space subjected to axial, lateral, and rotational loading. Folias [19] calculated the stress fields in the neighborhood of the intersection of a cylindrical inclusion and a free surface under tension. Kasano *et al*. [20] obtained the stress fields in an infinite body having a rigid cylindrical inclusion of finite length using Dougall's harmonic stress functions and the Fourier transform. Rajapakse [21] solved the solution of an axially loaded rigid inclusion bonded to a non-homogeneous elastic half space. Oel and Frechette [22] calculated the stress distribution in a thin disc having a cylindrical inclusion. Argon [23] obtained an approximate solution for the stresses around a slender elastic rod or platelet in an infinite elastic solid under uniform strain at infinity based on the Eshelby inclusion concept [24, 25]. Using the prolate spheroid to simulate a transverse isotropic fiber based on the Eshelby method, Tandon and Weng [26] investigated the effect of aspect ratio on the effective elastic moduli of polymer composites. These results prompted us to study the single-fiber fragmentation test based on the Eshelby approach. In this study, the prolate spheroid was used to simulate a

* On sabbatical leave from National Tsing Hua University, Hsinchu, Taiwan.
‡ Author to whom correspondance should be addressed.

fiber in a polymer matrix. The fiber strength is related to the fiber length based on the Weibull distribution. The critical aspect ratio is related to the load transfer from the matrix to the fiber when the fiber tensile stress reaches the fiber strength. This study is part of the ongoing research at the National Institute of Standards and Technology on the application of high-performance polymeric composites in civil engineering structures.

2. Stress Analysis

As an introduction to our model, consider a single fiber of length $2c$ and diameter $2a$ embedded in a polymer matrix subjected to an applied uniaxial tension σ^A. Both fiber and matrix are assumed to be elastically isotropic materials, and their shear moduli and Poisson's ratios are μ^*, ν^* and μ, ν, respectively. The fiber/matrix interface is assumed to be perfectly bonded. Because the fiber length is greater than the diameter by a factor of at least 10, the fiber can be treated as a prolate spheroid. The prolate spheroid in the Cartesian coordinate system x_1, x_2, and x_3 is defined mathematically by

$$\frac{x_1^2 + x_2^2}{a^2} + \frac{x_3^2}{c^2} \leq 1 \tag{1}$$

The aspect ratio k is defined as c/a and is greater than unity for a prolate spheroid. According to the stress-strain relation of the pure matrix, the uniform elastic strain e_{ij}^A arising from the remotely applied stress σ^A is

$$e_{ij}^A = \begin{pmatrix} -\nu & 0 & 0 \\ 0 & -\nu & 0 \\ 0 & 0 & 1 \end{pmatrix} \frac{\sigma^A}{E} \tag{2}$$

where E is the Young's modulus of the matrix. We analyze the stress fields of the single fiber embedded in a polymer matrix using the Eshelby approach.

Eshelby [24, 25] solved the inclusion inhomogeneity based on the equivalent inclusion method. The magnitude of the stress is uniform in the prolate spheroid and decreases with increasing distance from the inclusion for $E^* > E$. In this analysis, we are interested in the maximum tensile stress, which is in the inclusion for $E^* > E$, where E^* is the Young's modulus of the fiber. The internal stress of the inclusion is given as

$$\begin{aligned} \sigma_{ij}^I &= \lambda\left(e_{kk}^C + e_{kk}^A - e_{kk}^T\right)\delta_{ij} + 2\mu\left(e_{ij}^C + e_{ij}^A - e_{ij}^T\right) \\ &= \lambda^*\left(e_{kk}^C + e_{kk}^A\right)\delta_{ij} + 2\mu^*\left(e_{ij}^C + e_{ij}^A\right) \end{aligned} \tag{3}$$

where λ, μ and λ^*, μ^* are the Lamé coefficients of matrix and inclusion, respectively. It is noted that the Einstein summation convention is used throughout this paper. The parameter, δ_{ij}, is the Kronecker delta. The constraint strain, e_{ij}^C, is related to the transformation strain or eigenstrain e_{ij}^T by

$$e_{ij}^C = S_{ijkl} e_{kl}^T \tag{4}$$

in which the Eshelby tensor S_{ijkl} is a function of a and c, and the elastic constants of the matrix. Because of ellipsoid of revolution, e_{ij}^T can be written as

$$e_{ij}^A = \begin{pmatrix} e_{11}^T & 0 & 0 \\ 0 & e_{11}^T & 0 \\ 0 & 0 & e_{33}^T \end{pmatrix} \tag{5}$$

in which e_{11}^T and e_{33}^T are a function of the aspect ratio, the elastic constants of both the matrix and the inclusion, and the remote applied stress σ^A. Substituting Equation 4 into Equation 3, we obtain

$$e_{11}^T = \frac{(1-2\nu)\sigma^A}{2\mu} T_{11} \tag{6}$$

$$e_{33}^T = \frac{(1-2\nu)\sigma^A}{2\mu} T_{33} \tag{7}$$

where T_{11}, T_{33}, and relevant parameters are given in Appendix I. The stresses in the inclusion can be obtained from Equations 3, 6, and 7,

$$\sigma_{11}^I = \sigma^A\{[S_1(k) - 1]T_{11} + [R_1(k) - \nu]T_{33}\} \tag{8}$$

$$\begin{aligned} \sigma_{33}^I = \sigma^A\{&2[P_1(k) - \nu]T_{11} \\ &+ [Q_1(k) - 1 + \nu]T_{33} + 1\} \end{aligned} \tag{9}$$

in which

$$P_1(k) = \nu(S_{1111} + S_{1122}) + (1-\nu)S_{3311} \tag{10a}$$

$$Q_1(k) = 2\nu S_{1133} + (1-\nu)S_{3333} \tag{10b}$$

$$R_1(k) = S_{1133} + \nu S_{3333} \tag{10c}$$

$$S_1(k) = S_{1111} + S_{1122} + 2\nu S_{3311} \tag{10d}$$

where S_{ijkl} are expressed in Appendix I.

If the Poisson's ratio of the fiber is the same as that of the polymer matrix, the stresses in the inclusion can be reduced to

$$\sigma_{11}^I = -m\sigma^A[U_{11} + \nu U_{33}] \tag{11}$$

$$\sigma_{33}^I = -m\sigma^A[2\nu U_{11} + (1-\nu)U_{33}] \tag{12}$$

in which

$$U_{11} = \{\nu - (1-m)R_1(k)\}/U \tag{13}$$

$$U_{33} = \{(1-m)S_1(k) - 1\}/U \tag{14}$$

$$\begin{aligned} U = &2[(1-m)P_1(k) - \nu][\nu - (1-m)R_1(k)] \\ &+ [(1-m)Q_1(k) - 1 + \nu][(1-m)S_1(k) - 1] \end{aligned} \tag{15}$$

$P_1(k)$, $Q_1(k)$, $R_1(k)$, and $S_1(k)$ are defined in Equation 10, and the shear moduli ratio m is defined in Equation A3g. Several special cases are presented as follows. When $\nu = 1/3$, Equations 11 and 12 are the same as the counterparts derived by Shibato and Ono

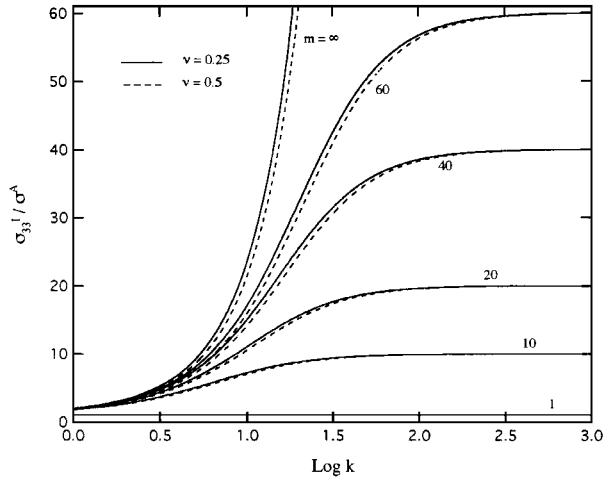

(a)

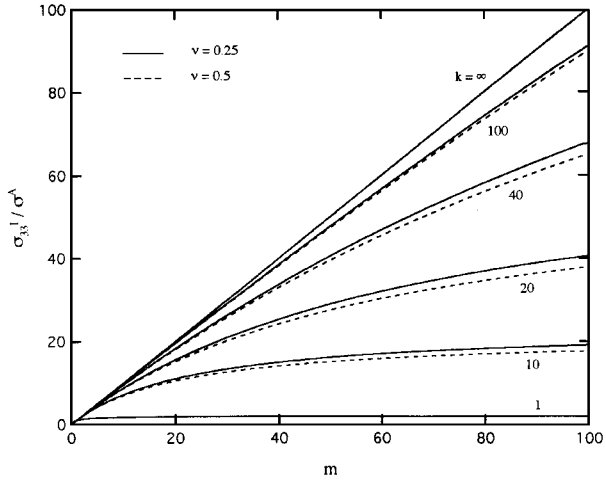

(b)

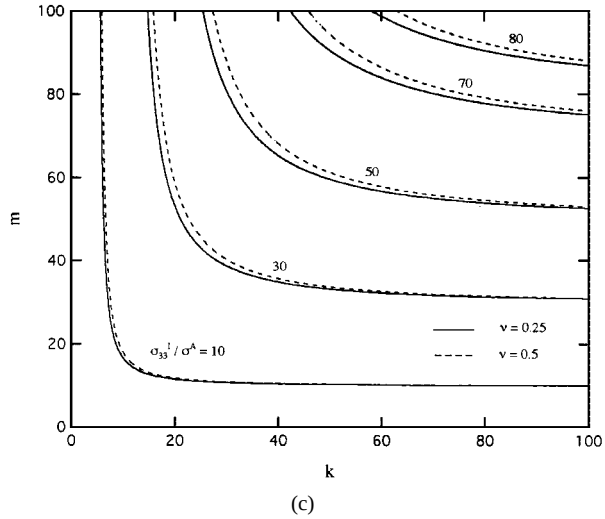

(c)

Figure 1 (a) σ_{33}^I/σ^A as a function of k; (b) σ_{33}^I/σ^A as a function of m; and (c) m as a function of k. Solid and dashed lines represent $\nu = \nu^* = 0.25$ and 0.5, respectively.

[27]. When m approaches unity ($\mu = \mu^*$), $M = -1/3$ (see Appendix II for the proof) and therefore $\sigma_{33}^I = \sigma_A$ and $\sigma_{11}^I = 0$, respectively. When k approaches infinity, σ_{33}^I becomes $m\sigma^A$.

Fig. 1a presents the relation between σ_{33}^I/σ^A and k for various values of m. This figure was obtained by assuming that both matrix and fiber have the same Poisson's ratio. Solid and dashed lines represent $\nu = \nu^* = 0.25$ and 0.5, respectively. It is found that σ_{33}^I/σ^A increases rapidly with $\log k$ to reach a plateau and approaches m. σ_{33}^I/σ^A is equal to unity for $m = 1$ regardless of k because both spheroid and matrix have the same physical properties. Comparing the solid and dashed lines, σ_{33}^I/σ^A is slightly greater for smaller values of Poisson's ratio than for larger ones for a given value of k. Fig. 1b plots σ_{33}^I/σ^A as a function of m with parameter k. The solid and dashed lines represent $\nu = \nu^* = 0.25$ and 0.5, respectively. σ_{33}^I/σ^A increases with m for a given value of k. In this case, σ_{33}^I/σ^A decreases slightly with increasing Poisson's ratio. Fig. 1c plots m as a function of k with parameter σ_{33}^I/σ^A. Again, the solid and dashed lines correspond to $\nu = \nu^* = 0.25$ and 0.5, respectively. The value of m decreases rapidly with increasing k and approaches σ_{33}^I/σ^A as k approaches infinity.

The effect of the matrix Poisson's ratio ($\nu^* \neq \nu$) on the relationship among axial stress, aspect ratio, and ratio of shear modulus is shown in Fig. 2, where the Poisson's ratio of the fiber is $\nu^* = 0.25$. Solid, dotted, and dashed lines correspond to $\nu = 0.25$, 0.37, and 0.5, respectively. The curves of σ_{33}^I/σ^A versus $\log k$ are given in Fig. 2a. For a given value of k or m, σ_{33}^I/σ^A decreases with increasing ν. For a given m, the difference of σ_{33}^I/σ^A between two matrix Poisson's ratios increases with increasing k. When the aspect ratio approaches infinity, the axial stress becomes

$$\sigma_{33}^I = \frac{m(1-\nu^*-2\nu\nu^*)}{(1+\nu)(1-2\nu^*)}\sigma^A \tag{16}$$

The effect of the matrix Poisson's ratio on the curves of σ_{33}^I/σ^A versus m is shown in Fig. 2b. For a given k, the difference of σ_{33}^I/σ^A between two matrix Poisson's ratios increases with increasing m. It is possible that, for a given m, σ_{33}^I/σ^A is larger for smaller k. The curves of m versus k for different σ_{33}^I/σ^A and ν are plotted in Fig. 2c. For a given k and σ_{33}^I/σ^A, m increases with increasing ν. If σ_{33}^I/σ^A remains constant, the difference of m between two matrix Poisson's ratios increases with decreasing k.

3. Fiber fragmentation

If the fiber is perfect, the theoretical cohesive strength is approximately equal to E^*/π where E^* is the Young's modulus of the fiber [28]. However, according to Griffith [29], because the fiber has flaws its tensile strength is much lower than the theoretical cohesive strength of a fiber having no defects. The data of tensile strength versus the diameter, $2a$, of a glass fiber having a 15.24 cm length given by Griffith [29] was fit by the solid line in Fig. 3, using the least-square curve-fitting method. The line is expressed by the following equation,

$$\sigma_{th} = 0.1544 + 0.01727/(2a) \tag{17}$$

where the units of σ_{th} and $2a$ are GPa and mm, respectively. In addition to the fiber diameter, the tensile strength of the fiber is also a function of its length. For example, data for the tensile strength of an AS4 fiber

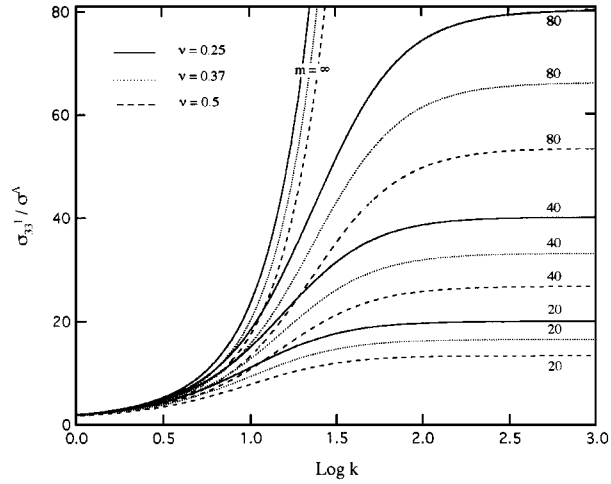

(a)

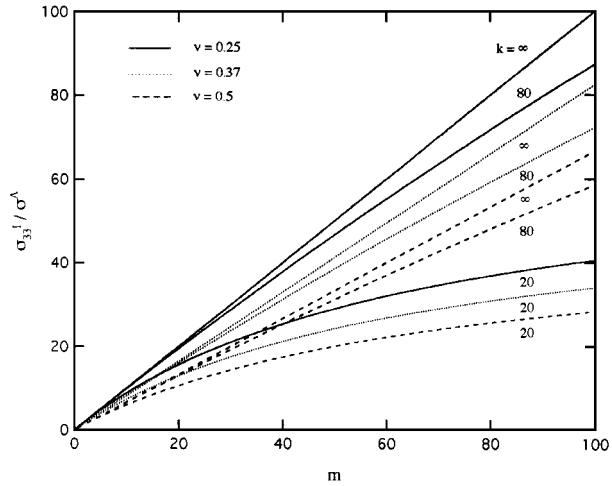

(b)

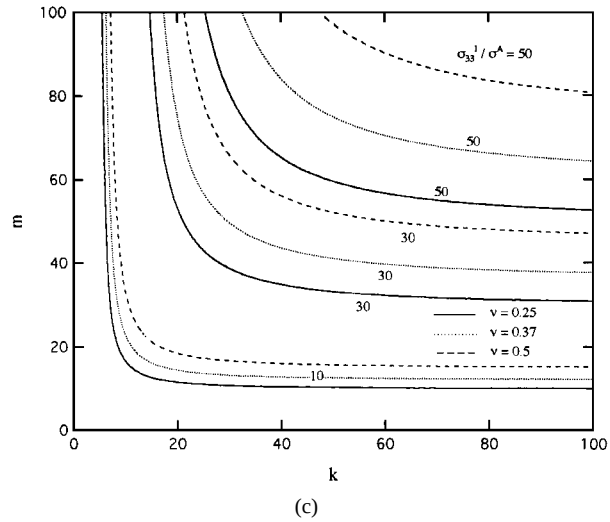

(c)

Figure 2 Effect of Poisson's ratio of matrix for: (a) σ_{33}^I/σ^A versus $\log k$; (b) σ_{33}^I/σ^A versus m; and (c) m versus k. Solid, dotted, and dashed lines correspond to $\nu = 0.25$, 0.37, and 0.5, respectively.

having a diameter of 6 μm versus fiber length, as measured by Waterbury and Drzal [30], are plotted as the dashed line in Fig. 3 and can be fit by the following equation using the least-square fitting method,

$$\log \sigma_{th} = -0.149 \log(2c) + 0.718 \qquad (18)$$

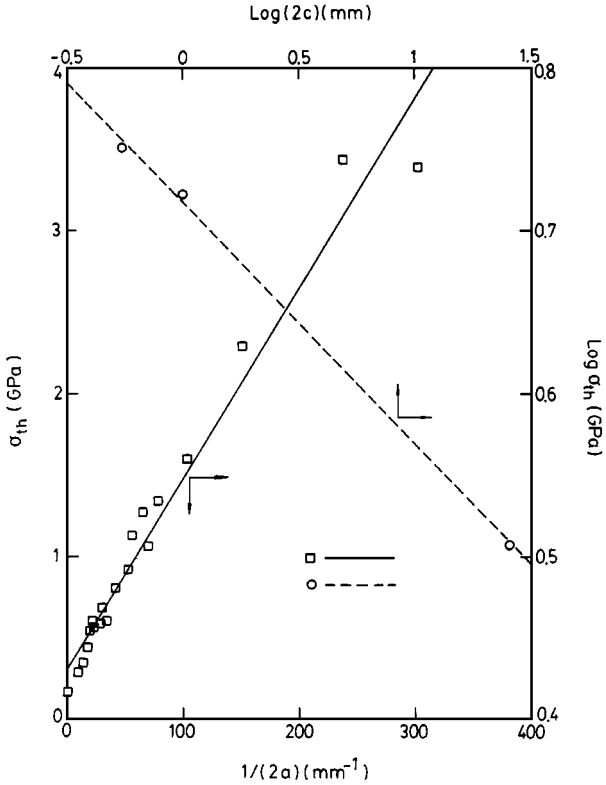

Figure 3 Effect of fiber diameter and length on fiber tensile strength. Solid line: tensile strength versus diameter, according to the experimental data obtained from [26]; dashed line: tensile strength versus gauge length, according to the experimental data obtained from [30].

where the units of σ_{th} and $2c$ are in GPa and mm, respectively. Equation 18 can be obtained by the Weibull probability of failure [7, 9]. Therefore, the tensile strength of fiber is inversely proportional to its diameter and length.

The fiber embedded in the polymer fractures when the maximum normal stress reaches the local tensile strength of the fiber. According to the above stress analysis, the maximum normal stress is the axial stress in the fiber. The axial stress increases with the applied stress, according to Equation 12. Therefore, the single fiber in the matrix fractures according to the following equation,

$$\sigma_{33}^I = \sigma_{th}(a, c) \qquad (19)$$

Using Equations 12 and 19, we obtain the applied stress to fracture the single fiber, σ_f^A, of a given size embedded in the polymer matrix as

$$\sigma_f^A = \sigma_{th}(a, c)/\{2[P_1(k) - \nu]T_{11} + [Q_1(k) - 1 + \nu]T_{33} + 1\} \qquad (20)$$

Fig. 4 displays plots of σ_f^A versus k for different values of ν and m using Equation 20 where $\sigma_{th}(a, c)$ is given by Equation 18 for $a = 3$ μm. The solid line for $\nu = 0.35$ is calculated using values of $\nu = 0.35$, $\nu^* = 0.25$, and $m = 68.5$, given by [30]. The other solid lines are calculated using the different matrix Poisson's ratios $\nu = 0.25$ and 0.5. It is found that σ_f^A decreases

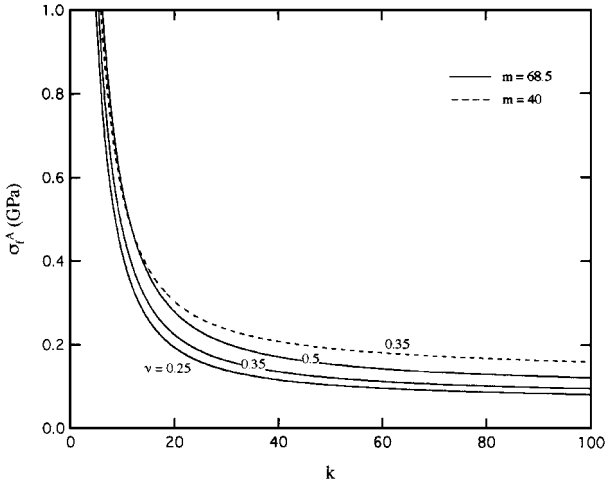

Figure 4 Applied stress at fiber fracture as a function of aspect ratio k. Solid and dashed lines correspond to $m = 68.5$ and 40, respectively, Poisson's ratio of fiber $\nu^* = 0.25$.

rapidly with increasing k. Further, for a given k, σ_f^A increases with increasing matrix Poisson's ratio. The dashed line is for the cases $m = 40$ and $\nu = 0.35$. Comparing both solid and dashed lines for the same matrix Poisson's ratio, we find that, for a given k, σ_f^A increases with decreasing ratio of shear modulus of fiber to matrix.

According to Fig. 4, for a given σ_{th}, σ_f^A increases with decreasing k. It is implied that the fiber in the polymer can fracture at any aspect ratio if the external stress is large enough. However, the stresses in the fiber as expressed in Equations 11 and 12 is valid only if the applied load can be transferred from the matrix to the fiber. When the aspect ratio decreases to a certain value, σ_f^A will no longer increase (or Equations 11 and 12 cannot be used anymore). This value is the so-called critical aspect ratio. According to Fig. 4, if σ_{th}/σ_f^A is constant, the critical aspect ratio decreases with increasing m. Netravali *et al*. [4] used the same carbon fiber embedded in different epoxies to study the single-fiber fragmentation test. Values of k and m used for Netravali's fiber/matrix systems are presented in Table I. Because the fiber was the same for all tests, σ_{th}/σ_f^A can be considered to be roughly constant. With the exception of the very flexible epoxy (see Table I), their critical aspect ratio decreased with increasing m. This is in qualitative agreement with our prediction.

TABLE I Fiber fragmentation aspect ratio of carbon fiber in different epoxies [4]

Strain rate	Epoxy	k	m
0.004 mm^{-1}	#1	92.68	171.6
	#2	93.09	172.6
	#3	88.64	182.9
	#4	84.90	222.4
	#5	71.34	410
	#6	103.72	517
0.007 mm^{-1}	#1	92.96	171.6
	#2	93.27	172.6
	#3	87.72	182.9
	#4	83.13	222.4
	#5	79.45	410
	#6	117.02	517

The effective interfacial shear strength, τ_c, is defined as the local fracture stress at the breaking point divided by twice the critical aspect ratio [1],

$$\tau_c = \frac{\sigma_{th}(k_c)}{2k_c} \tag{21}$$

As stated in the Introduction, the fiber length for the conventional single-fiber fragmentation test is long enough to break into more than twenty pieces. The two nearest fibers are able to interact with each other so that the stress state in the system is changed. In addition, such a long fiber is possible to allow defects on the interface. This complicated problem is very difficult to analyze the stress distribution, if not impossible. Therefore, we propose an alternative method in this paper to measure the critical aspect ratio and critical interfacial shear strength. A series of fibers of different lengths were prepared. If the fiber of a certain length embedded in the polymer is not broken under the tensile test, we increase the fiber length. The process is repeated until the fiber embedded in the polymer is broken. The minimum fiber length (or minimum aspect ratio) corresponding to the minimum tensile stress after the fiber broken is used to calculate the critical interfacial shear strength. Substituting σ^A by the minimum tensile stress in Equation 12, we obtain $\sigma_{th}(k_c)$. Then, substituting k_c by minimum aspect ratio in Equation 21, we get the critical interfacial shear strength. It should be noted that, in addition to neglecting the residual thermal stress, the above analysis was based on the assumption that both the fiber and matrix are isotropic materials. Obviously, an analysis for anisotropic properties could be performed but would be more complicated. Experiments using fibers having different lengths and diameters are being conducted to verify the model.

Netravali and co-workers [5, 6] measured the interfacial shear strengths of different fibers embedded in the same epoxy matrix using the acoustic emission technique. Their results are given in Table II. The first three rows are from [5] and last two rows are from [6]. Table II also includes the fiber strength, σ_f, given by commercial sources [31]. Based on these data, the ratio of $\sigma_{th}(k_c)$ to the cohesive strength is close to 0.1 with the exception of the second row. The local fracture stress $\sigma_{th}(k_c)$ is greater than the tensile strength provided by the commercial source because, according to the Weibull probability of failure, k_c is smaller than the gauge length commonly used for tensile testing. Therefore, it is possible to use the following empirical equation to predict the local tensile strength of a fiber embedded in the polymer matrix,

$$\sigma_{th} = 0.1E^*/\pi \tag{22}$$

4. Discussion

In this study, the prolate spheroid is used to simulate a cylindrical fiber. Argon [23] assumed both fiber and matrix have the same Poisson's ratio and obtained the

TABLE II Mean aspect ratio k_c, mean fragmentation length c_c, interfacial shear strength τ_c, Young's modulus of fiber E^*, the local fracture stress σ_{th}, and the ratio of σ_{th} to E^*/π, $r = \sigma_{th}/(E^*/\pi)$

Fiber	k_c	c_c (mm)	τ_c (MPa)	σ_{th} (GPa)	E^* (GPa)	r (GPa)	σ_f (GPa)
AS-4 graphite	62.04	0.46	60.26	7.48	210	0.11	2.5
S-2 glass	55.62	0.51	49.26	5.48	88	0.20	4.6
Kevlar	42.86	11.95	43.88	3.76	124	0.10	2.758
E-glass	42.93	0.97	27.50	2.36	77	0.10	2.1
E-glass	44.88	0.96	26.30	2.36	77	0.10	2.1

Note that σ_f was obtained from a commercial source [31].

axial stress at the end of fiber in matrix as

$$\sigma_{33}^{Ar} = \frac{1+\alpha k}{m+\alpha k} m\sigma^A \tag{23}$$

in which

$$\alpha = 4(1-\nu)/(3-2\nu-4\nu^2) \tag{24}$$

Kim *et al*. [15] considered a single fiber of radius a and length $2c$ embedded at the center of a coaxially cylindrical shell of matrix with an outer radius b. They obtained the axial stress at the center of fiber as

$$\sigma_{33}^{k} = \frac{1+\gamma}{m+\gamma}\left[1 - \frac{1}{\cosh(\beta_2 c)}\right] \tag{25}$$

in which

$$\gamma = a^2/(b^2-a^2) \tag{26a}$$

$$\beta_2^2 = \frac{(b^2-a^2)(1+m/\gamma)}{(1+\nu)[b^4\ln(b/a) - (b^2-a^2)/2 - (b^4-a^4)]} \tag{26b}$$

Fig. 5 displays a comparison of the axial stress obtained by the present study with those provided by the literature for $m = 60$. The solid, dotted, and dashed lines are from our model, Argon's [23], and Kim *et al*.'s [15] models, respectively. As k approaches infinity, all curves are equal to $60\,(=m)$. It is noted that the stress obtained by Argon is lower than that obtained by our study for large $\log k$ and the stress determined by Kim *et al*. shifts to the right when b/a increases. At $b/a = 100$, the stress obtained by Kim *et al*. is the closest to that obtained in this study. For fibers with an aspect ratio $b/a < 10$, as in the case of strong fiber/matrix interface, the present treatment starts to deviate from the true solutions. In such a case, this analysis cannot be used to predict the interfacial properties. Moreover, the true stress fields inside the fiber, as well as at the interface, are not considered by the current treatment. They may be solved by other methods, such as finite element analysis.

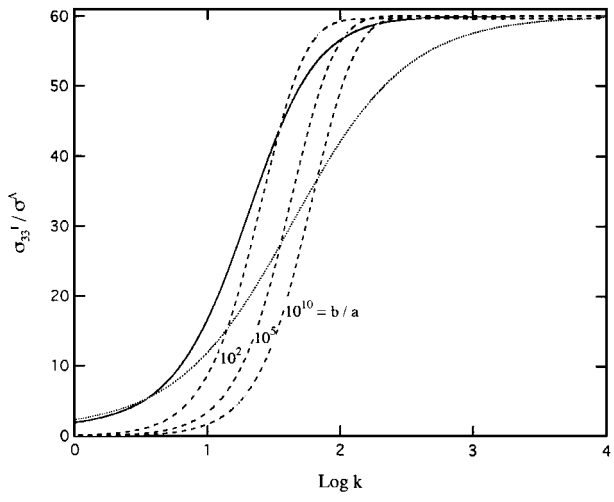

Figure 5 Comparison of axial stress for a fiber embedded in a polymer matrix obtained by the present study and literature. Solid line: axial stress on the fiber obtained by the present study; dotted line: axial stress at the fiber end obtained by Argon [23]; dashed lines: axial stress at the fiber center obtained by Kim *et al*., [15].

It should be emphasized that most analyses of the single-fiber fragmentation test are based on the Weibull distribution of failure using the expression:

$$P = 1 - \exp\left[-\left(\frac{c}{c_o}\right)\left(\frac{\sigma-\sigma_u}{\sigma_o}\right)^{\beta}\right] \tag{27}$$

in which P is the cumulative probability of failure of fiber of length $2c$ at stress σ, β is a shape parameter (Weibull modulus), σ_o is a scaling parameter associated with the fiber length $2c_o$, and σ_u is a threshold stress below which the failure probalility is zero. However, Asloun *et al*. [32] found that the Weibull distribution did not adequately describe the length dependence of the fiber strength in the single-fiber composite test. Further, the fracture stress, σ, at the fiber critical aspect ratio for a single-fiber fragmentation specimen has been often derived from [30, 33] to be

$$\sigma = \sigma^A E^*/E \tag{28}$$

where σ^A is the applied stress as defined earlier. According to our analysis, Equation 28 is valid when the aspect ratio of the fiber, k, is infinity and the Poisson's ratios of both the fiber and the matrix are the same, so that $m = E^*/E$, with $\sigma = m\sigma^A$ (see Fig. 1a). That is, Equation 28 generally over-estimates the fracture stress at the critical aspect ratio of the fiber or at later stages in a single-fiber fragmentation test.

5. Conclusions

A model for the single-fiber fragmentation test has been proposed. The fiber is approximated by a prolate spheroid. Under the action of an applied stress, normal stresses in the prolate spheroid embedded in a matrix of different elastic moduli are obtained using the Eshelby approach. The maximum normal stress is the

axial stress σ_{33}^I in the spheroid. The axial stress σ_{33}^I/σ^A in the spheroid increases with the aspect ratio, k, of the spheroid and the ratio of shear modulus of fiber to matrix, m. The value of k decreases with increasing m for a fixed σ_{33}^I/σ^A. The value of σ_{33}^I/σ^A decreases with increasing Poisson's ratios of matrix and fiber, for a given m or k, but m increases with increasing Poisson's ratios of matrix and fiber for a given k and σ_{33}^I/σ^A. Using this approach, the fracture stress of a single fiber/polymer matrix composite was analyzed. The analysis was based on the assumption that the tensile strength of the fiber is inversely proportional to its diameter and length. The applied stress at fiber fracture decreases monotonically with increasing aspect ratio of the broken fiber. For a given aspect ratio of broken fiber, the applied stress at fiber fracture increases with Poisson's ratios of fiber and matrix but decreases with increasing m. The critical aspect ratio is determined by the maximum aspect ratio at which the load cannot be transferred from matrix to fiber. The application of this model for determining the shear strength of fiber/polymer matrix composites is being investigated.

Appendix I

The parameters T_{11} and T_{33} are

$$T_{11} = \left[m - 1 + \frac{m(\nu^* - \nu)}{(1-2\nu^*)(1+\nu)}\right] \cdot \frac{\nu - R(k,m)}{2[P(k,m)-\nu][\nu - R(k,m)] + [S(k,m)-1][Q(k,m)-1+\nu]} \tag{A1a}$$

$$T_{33} = \left[m - 1 + \frac{m(\nu^* - \nu)}{(1-2\nu^*)(1+\nu)}\right] \cdot \frac{S(k,m) - 1}{2[P(k,m)-\nu][\nu - R(k,m)] + [S(k,m)-1][Q(k,m)-1+\nu]} \tag{A1b}$$

in which

$$P(k,m) = \left[\nu - \frac{m\nu^*(1-2\nu)}{1-2\nu^*}\right](S_{1111} + S_{1122}) + \left[1 - \nu - \frac{m(1-\nu^*)(1-2\nu)}{1-2\nu^*}\right]S_{3311} \tag{A2a}$$

$$Q(k,m) = 2\left[\nu - \frac{m\nu^*(1-2\nu)}{1-2\nu^*}\right]S_{1133} + \left[1 - \nu - \frac{m(1-\nu^*)(1-\nu)}{1-2\nu^*}\right]S_{3333} \tag{A2b}$$

$$R(k,m) = \left[1 - \frac{m(1-2\nu)}{1-2\nu^*}\right]S_{1133} + \left[\nu - \frac{m\nu^*(1-2\nu)}{1-2\nu^*}\right]S_{3333} \tag{A2c}$$

$$S(k,m) = \left[1 - \frac{m(1-2\nu)}{1-2\nu^*}\right](S_{1111} + S_{1122}) + 2\left[\nu - \frac{m\nu^*(1-2\nu)}{1-2\nu^*}\right]S_{3311} \tag{A2d}$$

$$S_{1111} = S_{2222} = \frac{3}{8(1-\nu)}\left[1 - \frac{1+3M}{2(k^2-1)}\right] + \frac{1-2\nu}{4(1-\nu)}(1+M) \tag{A3a}$$

$$S_{1122} = \frac{1}{8(1-\nu)}\left[1 - \frac{1+3M}{2(k^2-1)}\right] - \frac{1-2\nu}{4(1-\nu)}(1+M) \tag{A3b}$$

$$S_{1133} = S_{2233} = \frac{1}{4(1-\nu)}\frac{k^2(1+3M)}{k^2-1} - \frac{1-2\nu}{4(1-\nu)}(1+M) \tag{A3c}$$

$$S_{3311} = S_{3322} = \frac{1+3M}{4(1-\nu)(k^2-1)} + \frac{(1-2\nu)M}{2(1-\nu)} \tag{A3d}$$

$$S_{3333} = \frac{1}{2(1-\nu)}\left[1 - \frac{k^2(1+3M)}{k^2-1}\right] - \frac{(1-2\nu)M}{2(1-\nu)} \tag{A3e}$$

$$M = \frac{1}{k^2-1} - \frac{k}{(k^2-1)^{3/2}}\cosh^{-1}(k) \tag{A3f}$$

$$m = \frac{\mu^*}{\mu} \tag{A3g}$$

After suitable replacement, the expressions of S_{ijkl} are the same as those derived by Tandon and Weng [26]. According to the Eshelby tensor, S_{ijkl} is a non-dimensional parameter. However, Lee *et al*. [34] have reported that S_{ijkl} is proportional to the reciprocal of shear modulus. S_{3311} (= S_{3322}) is not equal to S_{1133} (= S_{2233}), but Lee and co-workers [34] have treated the two quantities as the same, that is, $S_{3311} = S_{1133}$.

Appendix II

Assume a function

$$M = \frac{1}{k^2-1} - \frac{k}{(k^2-1)^{3/2}}\cosh^{-1}(k)$$

Show that if k approaches unity, then $M = -1/3$. Proof:

$$
\begin{aligned}
M &= \lim_{k->1} \left\{ \frac{1}{k^2-1} - \frac{k}{(k^2-1)^{3/2}} \cosh^{-1}(k) \right\} \\
&= \lim_{k->1} \left\{ \frac{1}{k^2-1} - \frac{k}{(k^2-1)^{3/2}} \right. \\
&\quad \left. \times \tanh^{-1} \left[\frac{(k^2-1)^{1/2}}{k} \right] \right\} \\
&= \lim_{k->1} \left\{ \frac{1}{k^2-1} - \frac{k}{(k^2-1)^{3/2}} \left[\frac{(k^2-1)^{1/2}}{k} \right. \right. \\
&\quad \left. \left. + \frac{1}{3} \frac{(k^2-1)^{3/2}}{k^3} + \ldots . \right] \right\} \\
&= \lim_{k->1} \left\{ -\frac{1}{3k^2} + \ldots . \right\} \\
&= -\frac{1}{3}
\end{aligned}
$$

References

1. A. KELLY and W. R. TYSON, *J. Mech. Phys. Solids* **13** (1965) 329.
2. L. T. DRZAL, *SAMPE J.* **19** (1983) 7.
3. L. T. DRZAL, M. J. RICH, J. D. CAMPING and W. J. PARK, "Interfacial Shear Strength and Failure Mechanisms in Graphite Fiber Composites," Paper 20-C, 35th Annual Technical Conference, Reinforced Plastics/Composites Institute (The Society of the Plastics Industry, 1980).
4. A. N. NETRAVALI, R. B. HENSTENBURG, S. L. PHOENIX and P. SCHWARZ, *Polymer Comp.* **10** (1989) 226.
5. A. N. NETRAVALI, Z. F. LI, W. SACHSE and H. F. WU, *J. Mat. Sci.* **26** (1991) 6631.
6. A. N. NETRAVALI, L. T. T. TOPOLESKI, W. H. SACHSE and S. L. PHOENIX, *Comp. Sci. and Techn.* **35** (1989) 13.
7. L. M. ZHOU, J. K. KIM, C. BAILLIE and Y. W. MAI, *J. Comp. Mat.* **29** (1995) 881.
8. J. K. KIM and Y. W. MAI, *J. Mat. Sci.* **30** (1995) 3024.
9. L. H. PEEBLES, "Carbon Fibers: Formation, Structure, and Properties" (CRC Press, Boca Raton, Florida, 1995) Chap. 6.
10. J. SCHULTZ and M. NARDIN, *J. Adhesion* **45** (1994) 59.
11. M. NARDIN and J. SCHULTZ, *Composite Interfaces* **1** (1993) 113.
12. H. L. COX, *Brit. J. Appl. Phys.* **3** (1952) 72.
13. J. M. WHITNEY and L. T. DRZAL, "Axisymmetric Stress Distribution Around an Isolated Fiber Fragment". Toughened Composites, ASTM STP 937, edited by Norman J. Johnson (American Society for Testing and Materials, Philadelphia, 1987) pp. 179–196.
14. H.-Y. LIU, Y. W. MAI, L. M. ZHOU and L. YE, *Comp. Sci. and Techn.* **52** (1994) 253.
15. J. K. KIM, L. M. ZHOU and Y. W. MAI, *J. Mat. Sci.* **28** (1993) 6233.
16. A. N. GENT and C. WANG, *ibid.* **27** (1992) 2539.
17. H.-Y. LIU, Y. W. MAI, L. YE and L. M. ZHOU, *ibid.* **32** (1997) 633.
18. A. P. S. SELVADURAI and R. K. N. D. RAJAPAKSE, *Int. J. Solids Structures* **21** (1985) 1213.
19. E. S. FOLIAS, *Int. J. Fract.* **39** (1989) 25.
20. H. KASANO, H. MATSUMOTO and I. NAKAHARA, *Bull. of the JSME* **24** (1981) 1521.
21. R. K. N. D. RAJAPAKSE, *J. Engng Mech.* **116** (1990) 399.
22. H. J. OEL and V. D. FRECHETTE, *J. Am. Ceram. Soc.* **69** (1986) 342.
23. A. S. ARGON, *Fiber Sci. Tech.* **9** (1976) 265.
24. J. D. ESHELBY, *Solid State Phys.* **3** (1956) 79.
25. *Idem., Proc. Roy. Soc. London* **A241** (1957) 376.
26. G. P. TANDON and G. J. WENG, *Polym. Comp.* **5** (1984) 327.
27. M. SHIBATO and K. ONO, *J. Comp. Mats.* **12** (1978) 132.
28. R. W. HERTZBERG, "Deformation and Fracture Mechanics of Engineering Materials, 2nd Ed" (John Wiley, New York, 1983) p. 236.
29. A. A. GRIFFITH, *Philos. Trans. Royal Soc. London* **A221** (1921) 163.
30. M. C. WATERBURY and L. T. DRZAL, *J. Comp. Tech. and Research, JCTRER* **13** (1991) 22.
31. B. Z. JANG, "Advanced Polymer Composites" (ASM International, Materials Park, Ohio. 1994). Chap 2.
32. E. E. ASLOUN, J. B. DONNET, G. GUILPAIN, M. NADRIN and J. SCHULTZ, *J. Mat. Sci.* **24** (1989) 3504.
33. B. D. AGARWAL and L. J. BROUTMAN, "Analysis and Performance of Fiber Composites" (John Wiley, New York, 1980), p. 74.
34. J. K. LEE, D. M. BARNETT and H. I. AARONSON, *Metall. Trans.* **8A** (1977) 963.

Received 21 September 1997
and accepted 6 August 1998